Applied Chemical Engineering (2026) Volume 9 Issue 2 ISSN: 2578-2010 (O)
doi: 10.59429/ace.v9i2.5909

ORIGINAL RESEARCH ARTICLE

Green-synthesized MgO nanoparticles from *Gracilaria folifera*: Electrochemical and antidiabetic study

M. Adhithi[1], M. Yogeswari[1,*], K Dhanalakshmi[2], P. Sangeetha[3], M. Ehthishamul Haque[4], B. Sangeetha[5], S. Sivakumar[6], B. Esther Bharathi[6]

[1] *Department of Physics, Vellalar College for Women (Autonomous), Erode 638012, Tamil Nadu, India*

[2] *Department of Applied Sciences, New Horizon College of Engineering, Bengaluru 560103, Karnataka, India*

[3] *Department of Physics, Sona College of Technology, Salem 636005, Tamil Nadu, India*

[4] *Department of Physics, Sacred Heart College (Autonomous), Tirupattur 635601, Tamil Nadu, India*

[5] *Department of Electrical and Electronics Engineering, AVS Engineering College, Salem 636003, Tamilnadu, India*

[6] *Department of Physics, Government Arts College (Autonomous), Salem 636007, Tamilnadu, India*

Corresponding author: M. Yogeswari, m.yogeswari@vcw.ac.in

ABSTRACT

Magnesium oxide (MgO) nanoparticles are attractive materials for biomedical and electrochemical applications due to their defect-rich structure and high surface reactivity. In this study, MgO nanoparticles were synthesized using a green sol-gel method with *Gracilaria folifera* extract (GF-MgO) acting as a natural reducing and capping agent. Structural analysis confirmed the formation of phase-pure cubic MgO with nanoscale crystallite size. Spectroscopic studies revealed successful biofunctionalization and the presence of oxygen vacancies induced by algal biomolecules. Electrochemical investigations demonstrated quasi-reversible redox behavior with enhanced charge transfer properties. The biofunctionalized GF-MgO nanoparticles exhibited improved antidiabetic activity, showing lower IC_{50} values for α-amylase (37.06 µg/mL) and α-glucosidase (48.91 µg/mL) compared to pure MgO. The enhanced performance is attributed to synergistic interactions between MgO defect sites and *Gracilaria folifera* phytochemicals. This work highlights a simple and eco-friendly strategy for producing biofunctional MgO nanoparticles with improved electrochemical and therapeutic potential. This study presents a novel approach for synthesizing defect-engineered, biofunctional MgO nanoparticles using *Gracilaria folifera*, demonstrating the synergistic role of algal biomolecules in enhancing electrochemical performance and antidiabetic activity.

Keywords: MgO nanoparticles; *Gracilaria folifera*; green synthesis; biofunctionalization; defect engineering; oxygen vacancies; electrochemical behavior; antidiabetic activity

ARTICLE INFO

Received: 18 February 2026
Accepted: 23 April 2026
Available online: 15 May 2026

1. Introduction

Magnesium oxide (MgO) nanoparticles are an emerging class of multifunctional nanomaterials widely explored for biomedical, catalytic, optical and electrochemical applications[1]. Their inherent properties high melting point, large bandgap, strong ionic bonding, defect-rich lattice and ability to generate reactive oxygen species (ROS) make MgO nanostructures particularly attractive for antioxidant, antidiabetic, antimicrobial and anticancer activities[2]. Diabetes mellitus is a major global health concern characterized by chronic hyperglycemia and associated metabolic complications affecting vital organs such as the heart, kidneys, and nervous system. The increasing prevalence and mortality associated with diabetes highlight the urgent need for effective therapeutic strategies and advanced materials for

enzyme inhibition and glucose regulation. Conventional antidiabetic drugs often suffer from limitations such as side effects, reduced long-term efficacy, and poor selectivity, necessitating the development of alternative approaches. In this context, nanomaterials, particularly defect-engineered metal oxides, have emerged as promising candidates due to their tunable surface properties and enhanced biological interactions. The novelty of the present work lies in the integration of green synthesis and defect engineering using *Gracilaria folifera* extract, enabling the formation of biofunctionalized MgO nanoparticles with enhanced electrochemical activity and improved antidiabetic performance. At the nanoscale, MgO exhibits significantly enhanced reactivity due to the presence of oxygen vacancies (V_o), F-centers and surface defect states, which play a central role in electron transfer, catalytic activity and biological interactions[3].

Conventional chemical synthesis of MgO nanoparticles requires high temperatures, toxic reagents and harsh stabilizers, which can limit biocompatibility and pose environmental concerns[4]. Among various synthesis techniques, the sol-gel auto-combustion method offers significant advantages for the preparation of metal oxide nanoparticles. This method enables uniform mixing at the molecular level, leading to high phase purity and controlled stoichiometry. It facilitates the formation of nanoscale particles at relatively lower temperatures with improved homogeneity and reduced agglomeration. Moreover, the auto-combustion process promotes the generation of porous structures and defect-rich surfaces, which are beneficial for enhancing electrochemical activity and catalytic performance. These features make the sol-gel auto-combustion method particularly suitable for synthesizing defect-engineered MgO nanoparticles with improved functional properties. Green synthesis approaches offer a sustainable alternative by utilizing biological extracts that function as natural reducing, stabilizing and capping agents. Marine macroalgae have recently gained attention as highly efficient bio templates due to their rich composition of polysaccharides, alkaloids, phenolic compounds, proteins, terpenoids and sulfated biopolymers that facilitate controlled nucleation and surface modification of nanoparticles[5].

Gracilaria folifera, a red marine alga abundant along the Indian coastline, is particularly rich in agar, galactans, sulfated polysaccharides and antioxidant biomolecules[6]. These functional groups act as strong electron donors capable of reducing metal ions while simultaneously stabilizing the forming nanostructures through hydrogen bonding and electrostatic interactions. Their high density of hydroxyl, sulfate and carbonyl groups promotes efficient surface functionalization, prevents agglomeration and enhances particle stability[7]. Green-synthesized MgO using *Gracilaria folifera* offers not only improved biocompatibility but also modified physicochemical behaviour due to the synergistic interaction between the inorganic lattice and organic scaffold[8].

The bioorganic compounds can modulate defect formation, tune optical transitions and enhance electron transfer kinetics. This is supported by electrochemical findings where *G. folifera* modified MgO exhibits enhanced defect-mediated charge transfer and pseudocapacitive behaviour, attributed to the interaction between MgO oxygen vacancies and organic functional groups[9]. Such interactions increase electroactive surface area, accelerate heterogeneous electron transfer and stabilize intermediate oxidation states properties highly valuable for biomedical and electrochemical applications[10].

Recent studies have highlighted the importance of metal oxide nanomaterials in various functional applications, including catalysis, energy storage, and biomedical fields. In particular, MgO and related oxide systems exhibit tunable structural, electronic, and defect properties that significantly influence their performance[11-17].

MgO nanoparticles synthesized using biological extracts have shown strong antioxidant activity, primarily due to ROS scavenging ability and surface electron-donating groups. The antidiabetic activity of MgO is associated with inhibition of carbohydrate-degrading enzymes, possibly through chelation, surface adsorption and hydrogen-bond interactions facilitated by biogenic capping molecules. Moreover, MgO

nanoparticles can induce cancer cell apoptosis through ROS-mediated mitochondrial damage, DNA fragmentation and disruption of membrane integrity mechanisms strongly influenced by particle size, surface defects and phytochemical functionalization. Despite significant interest in green-synthesized MgO, very few studies have explored the use of *Gracilaria folifera*, especially in the context of biomedical applications. Its unique combination of polysaccharides and red-algae-specific metabolites offers distinct advantages in controlling the crystallinity, bandgap and biological activity of the synthesized nanoparticles.

Thus, the main contribution of this work includes:

- To synthesize defect-engineered magnesium oxide (MgO) nanoparticles using a green sol-gel method with *Gracilaria folifera* extract as a bio-reducing and capping agent.
- To investigate the structural, spectroscopic, and surface characteristics of the synthesized nanoparticles and analyze the role of biofunctionalization in defect formation.
- To evaluate the electrochemical performance of the biofunctionalized MgO nanoparticles, focusing on defect-assisted charge transfer and pseudocapacitive behavior.
- To assess the antidiabetic activity of the synthesized nanoparticles through enzyme inhibition studies and establish a correlation between defect chemistry and biological performance.

The synthesized defect-engineered MgO nanoparticles functionalized with *Gracilaria folifera* demonstrate significant potential for practical applications in both biomedical and electrochemical fields. The enhanced antidiabetic activity indicates their suitability for enzyme inhibition-based therapeutic applications, particularly in regulating postprandial glucose levels. In addition, the defect-induced pseudocapacitive behavior and improved charge transfer characteristics make these nanoparticles promising candidates for electrochemical sensors and energy storage devices. The presence of oxygen vacancies and bio-organic functional groups further enhances surface reactivity, enabling applications in catalysis and biomedical diagnostics. Therefore, the proposed green synthesis approach offers a multifunctional platform for developing advanced nanomaterials for healthcare and energy-related applications.

2. Experimental Methods and Materials

2.1. Materials and Collection of Marine Biomass

Fresh *Gracilaria folifera* seaweed was collected from the Gulf of Mannar biosphere reserve (9°15.623′ N, 79°5.539′ E; Indian Ocean inlet) on 16 August 2023**.** The biomass was thoroughly washed with seawater and subsequently with distilled water to eliminate epiphytes, salts, and debris. The cleaned samples were shade-dried, powdered, and stored in airtight containers for further extraction[18].

Analytical-grade magnesium nitrate hexahydrate ($Mg(NO_3)_2 \cdot 6H_2O$, 98%; NICE Chemicals Ltd., India) was used as the Mg precursor. Distilled water served as the solvent. Ethanol (C_2H_6O) was used during washing to remove unreacted residues. No additional surfactants or chemical stabilizers were used[19].

2.2. Synthesis Procedures

The synthesis pathways for both pure MgO nanoparticles and GF-MgO nanoparticles are illustrated in **Figure 1**, which outlines the sol-gel route for pure MgO and the phycogenic route utilizing *G. folifera* extract as a natural reducing and capping agent.

2.3. Preparation of Gracilaria folifera Extract

To extract the phytochemical-rich biofuel, 2 g of dried *G. folifera* powder was suspended in 100 mL of double-distilled water and heated at 60 °C with continuous stirring (720 rpm) for 1 h**.** The mixture was filtered

to obtain a clear aqueous extract containing polysaccharides, phenolics, flavonoids, proteins, and sulfated galactans. This extract acted as the reducing, stabilizing and capping agent for the green synthesis of MgO[20].

2.4. Synthesis of Pure MgO Nanoparticles

For comparison, pure MgO nanoparticles were synthesized through a sol-gel combustion route without any biological extract**.** A 0.5 M solution of $Mg(NO_3)_2 \cdot 6H_2O$ was prepared in distilled water and stirred at 50 °C for 1 h**.** Gelation occurred upon gradual evaporation, forming a thick nitrate gel. The gel was dried at 150 °C overnight, followed by calcination at 400 °C for 3 h to achieve phase-pure crystalline MgO. This control sample represents chemically derived MgO without biomolecular functionalization[21].

2.5. Synthesis of GF-MgO Nanoparticles

For the green synthesis, 0.5 M $Mg(NO_3)_2 \cdot 6H_2O$ was dissolved in 40 mL of *G. folifera* extract and stirred at 50 °C for 1 h. The precursor-extract mixture was ultrasonicated for 30 min to enhance Mg^{2+} dispersion and accelerate phytochemical-metal ion complexation. This was followed by an additional 1 h of stirring to initiate sol-gel formation. The sol was aged overnight for complete gelation, filtered, and washed thoroughly with distilled water and ethanol to remove excess organics.

The dried gel was subjected to controlled calcination at 400 °C for 3 h**,** during which the biopolymeric matrix decomposed, yielding defect-rich, biofunctionalized MgO nanoparticles. The *G. folifera* extract provides a rich combination of reducing species such as phenolics and sulfated polysaccharides, along with stabilizing and capping ligands including hydroxyl, carboxyl, and sulfate groups (-OH, -COOH, SO_4^{2-}), which collectively regulate nucleation, control morphology, and induce beneficial defect states, thereby producing a distinct organic-inorganic hybrid surface that is markedly different from pure MgO[22].

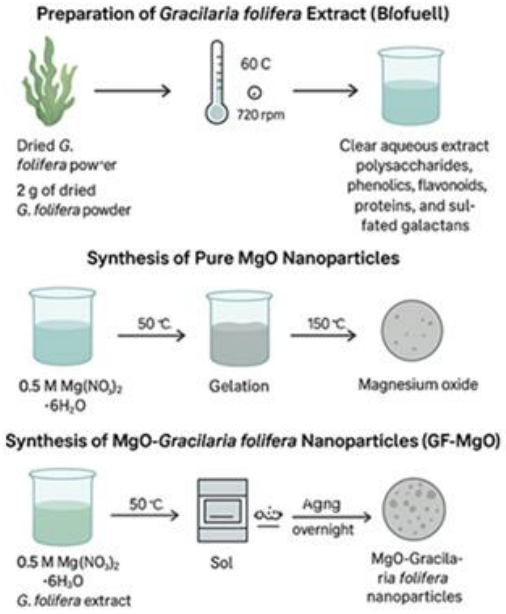

Figure 1. Schematic illustration of the synthesis pathways for pure MgO and GF-MgO nanoparticles.

2.6. Reaction Mechanism

The green synthesis involves reduction of Mg^{2+} ions mediated by phytochemicals such as hydroxyl and sulfate groups present in *Gracilaria folifera*. These functional groups coordinate with Mg^{2+} ions, forming intermediate complexes that undergo thermal decomposition during calcination to yield MgO nanoparticles. Simultaneously, the decomposition of organic constituents generates oxygen vacancies and stabilizes defect-rich structures.

All experiments were performed at least three times under identical conditions to ensure reproducibility. The synthesized nanoparticles were stored in airtight containers to prevent atmospheric contamination.

3. EXPERIMENTAL TECHNIQUES

The crystalline structure of pure MgO and GF-MgO nanoparticles was analyzed using X-ray diffraction (XRD) on a Bruker D2 Phaser diffractometer equipped with Cu Kα radiation (λ = 1.5406 Å), operated at 40 kV and 30 mA, over a 2θ range of 20°-80°. Fourier Transform Infrared (FTIR) spectra were recorded using a PerkinElmer Spectrum spectrometer in the range 4000-400 cm^{-1} (KBr pellet method) to identify functional groups and biomolecular interactions associated with *G. folifera* phytochemicals. Electrochemical properties of the GF-MgO-modified electrode were examined by Cyclic Voltammetry (CV) in 0.1 M phosphate buffer solution (PBS) containing the selected analyte using a standard three-electrode system. Surface elemental composition, oxidation states, and defect-related chemical features were characterized using X-ray photoelectron spectroscopy (XPS). Antidiabetic activity was evaluated through α-amylase and α-glucosidase inhibition assays, and the reaction absorbances were measured at 540 nm and 405 nm, respectively, using a UV-Visible spectrophotometer.

4. RESULT AND DISCUSSION

4.1. XRD Discussion

The X-ray diffraction pattern of MgO nanoparticles synthesized using *Gracilaria folifera* extract (**Figure 2**) shows a series of sharp and intense reflections at 2θ ≈ 36.8°, 42.8°, 62.1°, 74.5° and 78.3°, which correspond to the (111), (200), (220), (311) and (222) planes of cubic magnesium oxide with a rock-salt structure (JCPDS No. 89-7746). The dominant intensity of the (200) reflection indicates a mild preferential orientation along this crystallographic plane. The well-defined diffraction peaks confirm that the synthesized nanoparticles possess high crystallinity and a phase-pure MgO structure without any trace of secondary phases such as $Mg(OH)_2$, carbonates, or unreacted precursor salts. This purity strongly reflects the efficiency of *G. folifera* extract in promoting complete reduction, conversion, and crystallization of Mg^{2+} ions during the sol-gel process and subsequent calcination[23]. The weak diffraction peak observed near 2θ ≈ 28-29° does not correspond to the characteristic reflections of cubic MgO. This peak is attributed to trace amounts of residual $Mg(OH)_2$ (brucite phase) and/or surface magnesium carbonate species formed due to atmospheric CO_2 adsorption.

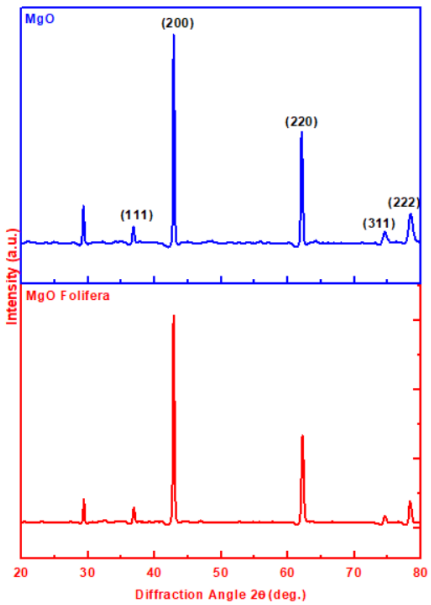

Figure 2. XRD pattern of MgO and GF-MgO nanoparticles.

The absence of additional peaks is attributed to the amorphous nature of biomolecules and decomposition of minor mineral components during calcination. Instead, any contribution from amorphous organics appears only as a broad background halo that becomes negligible after calcination. Likewise, while marine algae naturally contain small quantities of crystalline mineral salts such as potassium, calcium and sodium compounds, these elements are present in trace amounts and are largely volatilized, decomposed or transformed during heat treatment at 400 °C. Consequently, even though they contribute to the overall mass of the biomass, these mineral components do not produce characteristic peaks in the final XRD spectrum. The sharp and intense peaks observed in the pattern can therefore be attributed exclusively to the highly crystalline MgO phase[24].

The average crystallite size (D) of the synthesized MgO nanoparticles was calculated using the Debye-Scherrer equation:

$$D = \frac{K\lambda}{\beta cos\theta}$$

where

D - crystallite size, K - shape factor (typically 0.9), λ - wavelength of Cu Kα radiation (1.5406 Å), β - the full width at half maximum (FWHM) of the diffraction peak (in radians), and θ - Bragg diffraction angle.

The average crystallite size calculated using the Debye-Scherrer equation is 32.19 nm (**Table 1**), which aligns closely with the Williamson-Hall value of 31.42 nm, suggesting minimal microstrain and uniform crystal growth. Rietveld refinement further validates the structural identity with a refined lattice parameter of a = 4.2231 Å and a goodness-of-fit (GoF) value of 0.74, confirming excellent agreement between observed and simulated diffraction profiles. The calculated dislocation density (1.0×10^{-3} m^{-2}) indicates well-ordered crystallites with limited structural imperfections. Slight peak broadening, especially in the (111) and (220) reflections, may be attributed to nanoscale effects and the presence of intrinsic point defects such as oxygen vacancies and Mg interstitials, which are commonly generated during thermal decomposition of the precursor. These defect centers are beneficial because they influence the surface reactivity, optical absorption, bandgap energy and biological activity of MgO nanoparticles.

The phytochemical constituents of *Gracilaria folifera* play an essential role in controlling crystallization. Hydroxyl, carboxyl, sulfate and polysaccharide groups bind to Mg^{2+} ions during nucleation, modulating the

sol-gel transition and restricting uncontrolled grain growth. During calcination, the organic matrix decomposes, creating transient microchannels that favor the formation of uniformly sized crystallites and limit agglomeration. This bio-templating effect not only determines crystallite size but also stabilizes surface defect sites, which are known to enhance performance in antioxidant, antidiabetic, and anticancer applications[25]. Thus, the XRD results confirm that *G. folifera* extract is an effective green templating agent, yielding phase-pure, highly crystalline MgO nanoparticles with nanoscale crystallite dimensions and beneficial defect chemistry. The structural parameters extracted from XRD analysis, including crystallite size, lattice parameter, microstrain, and dislocation density, are summarized in **Table 1**.

Table 1. Structural parameters of GF-MgO nanoparticles obtained from XRD analysis.

Parameter	Symbol	Value	Unit	Method / Notes
Crystallite size (Scherrer)	D	32.19	nm	From (200) reflection
Crystallite size (W-H)	DW-H	31.42	nm	Size-strain analysis
Dislocation density	δ	1.0×10^{-3}	lines/m²	$\delta = 1 / D^2$
Microstrain	ε	2.5×10^{-3}	-	From slope of W-H plot
Lattice parameter	a_0	4.2231	Å	Rietveld refinement
Unit cell volume	V	75.3169	Å^3	Rietveld refinement
FWHM of major peak (200)	β	0.27	degree	After instrument correction
Space group	-	Fm3m	-	Cubic MgO
Goodness of fit	GoF	0.74	-	Rietveld refinement

Table 1. (*Continued*)

The extracted structural parameters confirm the formation of highly crystalline, nanoscale MgO with low microstrain and defect-controlled lattice characteristics, which are beneficial for enhanced electrochemical and biological performance. The slight peak and shift seen in GF-MgO when compared to MgO denote distortion in the crystal structure and decreased crystallite size owing to biofunctionalization. This suggests that phytochemicals from *Gracilaria folifera* interfere with crystal growth, leading to controlled nucleation and defect formation. These defects are responsible for increasing the reactivity of the surface and significantly enhance electrochemical charge transfer and enzyme reactions.

4.2. Fourier Transform Infrared Spectroscopy (FTIR) Analysis

The FTIR spectra of pure MgO and *Gracilaria folifera*-functionalized MgO (GF-MgO) provide critical insight into the organic-inorganic interfacial chemistry governing nanoparticle nucleation, stabilization, and defect evolution during the biogenic synthesis process (**Figure 3**). The chemically synthesized MgO exhibits a characteristic inorganic vibrational profile with minimal surface organic signatures, whereas the GF-MgO spectrum shows pronounced biomolecular fingerprints arising from polysaccharides, proteins, phenolics, and sulfated galactans inherent to *G. folifera*[26].

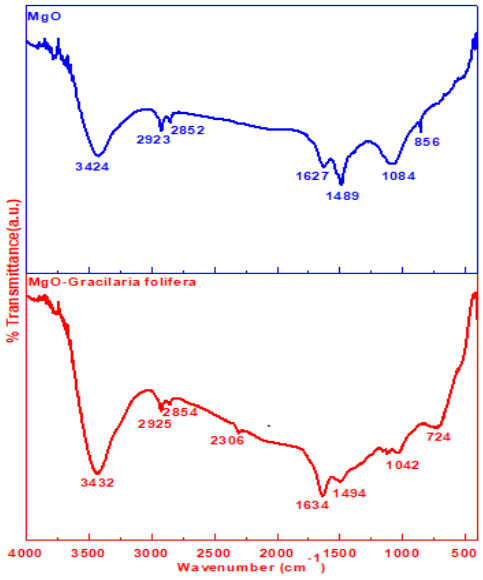

Figure 3. FTIR spectrum of MgO and MgO- GF-MgO nanoparticles.

4.2.1. Pure MgO Spectrum

Pure MgO displays a moderately weak and narrow O-H stretching band at 3424 cm^{-1}, arising from physisorbed moisture and isolated surface hydroxyl groups. The low intensity signifies a largely hydroxyl-deficient surface typical of thermally formed MgO with minimal residual hydration[27]. Weak bands at 2923 and 2852 cm^{-1} correspond to trace aliphatic C-H vibrations, likely originating from atmospheric hydrocarbons adsorbed during sample storage[28]. The bending mode at 1627 cm^{-1} reflects molecularly adsorbed water, confirming limited surface hydration[29].

The prominent absorption peaks at 1084 and 856 cm^{-1} correspond to Mg-O lattice vibrational modes of the cubic $Fm\bar{3}m$ rock-salt structure. The 856 cm^{-1} mode arises from Mg-O translational phonons, whereas the 1084 cm^{-1} band corresponds to asymmetric lattice distortions associated with surface defects[30]. Their sharpness confirms a highly crystalline, defect-poor structure. Overall, the FTIR profile of pure MgO is dominated by lattice vibrational modes and minimal organic interference, consistent with an inorganic oxide surface.

4.2.2. GF-MgO Spectrum

In contrast, the FTIR spectrum of GF-MgO demonstrates substantial modification due to the strong adsorption and coordination of algal biomolecules during the green synthesis process. The broad and intense O-H stretching envelope at 3432 cm^{-1} indicates extensive hydrogen bonding between hydroxyl-rich polysaccharides and surface -OH groups generated during $Mg(OH)_2 \rightarrow MgO$ conversion. This broadening is characteristic of complex hydrogen-bonded networks formed by sulfated galactans and agar-derived biopolymers. Although the FTIR spectrum of *Gracilaria folifera* extract was not recorded in this study, the functional group assignments are consistent with reported FTIR spectra of *Gracilaria* species and red algae, confirming the involvement of biomolecules in nanoparticle reduction and stabilization.

The enhanced C-H stretching modes at 2925 and 2854 cm^{-1}, absent in pure MgO, confirm the presence of long-chain aliphatic CH_2/CH_3 groups associated with lipid residues and carbohydrate backbones. A new intermediate-intensity band at 2306 cm^{-1}, not observed in pure MgO, is attributed to atmospheric CO_2 or weakly adsorbed species[31]. Its appearance indicates the incorporation of proteinaceous species or trace amino-functionalized polysaccharides.

The strong absorption at 1634 cm^{-1} corresponds to the amide I (C=O stretching) vibration of proteins and peptide linkages, while the band at 1494 cm^{-1} is associated with N-H deformation and aromatic ring vibrations from phenolics and flavonoids. These bands confirm chemisorption of proteinaceous and phenolic components onto the MgO surface.

The intense band at 1042 cm^{-1} represents C-O-C asymmetric stretching and C-O vibrations of sulfated galactans key structural polysaccharides in *G. folifera*[32]. This indicates that these polysaccharides function as capping and stabilizing agents, regulating nucleation, preventing aggregation, and promoting uniform crystallite formation.

Table 2. FTIR Peak Assignments for MgO and GF-MgO.

Wavenumber (cm^{-1})	Pure MgO	GF-MgO	Assignment	Technical Interpretation
3432-3424	Weak O-H	Strong, broad O-H	O-H stretching	Hydrogen-bonded networks; polysaccharides and hydration shell
2925-2923	Very weak	Strong	C-H (CH_2/CH_3)	Aliphatic chains from polysaccharides, lipids, proteins
2854-2852	Trace	Enhanced	C-H symmetric stretch	Increased organic capping layer thickness
2306	Absent	Present	CO_2 (adsorbed)	Nitrogenous metabolites, protein residues
1634-1627	Weak	Strong	Amide I (C=O), H-O-H	Protein binding to Mg^{2+}; water-biopolymer interactions
1494-1489	Weak	Strong	N-H, aromatic vibrations	Phenolics, flavonoids, aromatic amino acids
1042-1084	Weak	Strong	C-O-C, C-O stretching	Sulfated galactans, agar polysaccharides; strong capping effect
724-856	Strong Mg-O	Shifted Mg-O	Mg-O lattice vibration	Lattice distortion, Mg-O-C/S coordination, oxygen vacancies

A significant lattice mode shift is observed for the Mg-O phonon band, which moves from 856 cm^{-1} (pure MgO) to 724 cm^{-1} (GF-MgO) shown in **Table 2**. This redshift can be attributed to several synergistic effects arising from biogenic modification of the MgO lattice. The formation of surface Mg-O-C and Mg-O-S coordination complexes due to strong binding of bio-organic constituents from *G. folifera* alters the local chemical environment of lattice oxygen. This is accompanied by an increased density of oxygen-vacancy (V_o) sites and lattice distortion induced by organic-inorganic interfacial interactions. This shift indicates lattice distortion and increased defect density due to biofunctionalization.

The observed enhancement and broadening of O-H, C-H, and C-O bands confirm strong interaction between MgO nanoparticles and algal biomolecules. These functional groups act as active binding sites, facilitating surface adsorption and stabilization of nanoparticles. The shift in Mg-O vibrational frequency further indicates modification of the lattice environment due to organic-inorganic coupling, which contributes to increased defect density and improved catalytic and biological activity.

4.3. Cyclic Voltammetry Analysis

The cyclic voltammetric characteristics of *Gracilaria folifera*-functionalized MgO (GF-MgO) nanoparticles recorded in the potential range -0.20 to +0.20 V in 0.1 M phosphate buffer solution (PBS) containing H_2O_2 are shown in **Figure 4**. These voltammograms provide a detailed electrochemical signature of the defect-engineered oxide and its interaction with biopolymeric functional groups derived from the algae. The family of curves obtained at multiple scan rates displays a consistent anodic-cathodic peak pair centered at approximately -0.03 V and +0.04 V, whose magnitude, spacing, and evolution with scan rate reflect the underlying electron-transfer processes and the role of defect states introduced during green synthesis. The reproducibility of the voltammograms across the entire scan-rate range indicates that the GF-MgO electrode maintains structural and electrochemical stability, which is essential for high-rate charge-storage and electrocatalytic sensing systems[33].

The redox behavior is attributed to defect-mediated electron transfer and oxygen vacancy states. The presence of biogenic hydroxyl, sulfate, carbonyl, and polysaccharide groups modulates the electronic environment of MgO by altering local energy levels and providing additional redox-active sites. As a result, the reduction peak exhibits high current density and minimal kinetic hindrance, indicating facilitated electron uptake into MgO defect sites in the PBS-analyte system[34].

The increase in cathodic peak current with scan rate, accompanied by a minor negative shift, indicates quasi-reversible behavior. This trend highlights the involvement of singly ionized oxygen vacancies, surface hydroxyl-related traps, and partially reduced Mg^{+} centers, all of which contribute to the pseudocapacitive characteristics of the electrode. The anodic peak near +0.04 V corresponds to reoxidation of these reduced species and shows slightly broader features due to slower structural relaxation and vacancy annihilation. Between the redox peaks, the rising baseline current confirms strong surface-controlled pseudocapacitance, which remains dominant even at high scan rates.

Comparison with pure MgO confirms that the *G. folifera* functional layer significantly enhances electroactive surface area, wettability, and interfacial electron transfer for analytes such as H_2O_2. This improvement results in higher anodic and cathodic peak currents, lower overpotentials, and preserved current profiles even at high scan rates. The peak-to-peak separation of ~70 mV meets Laviron's criteria for quasi-reversible systems, corresponding to $k^0 \approx 10^{-2}$ cm s^{-1} and analyte diffusion coefficients of $\sim 10^{-5}$ cm^2 s^{-1}. The reduced hysteresis between forward and reverse scans highlights low internal resistance and efficient charge redistribution across the GF-MgO surface.

Moderate peak broadening at higher scan rates arises from multiple, energetically distinct redox-active sites rather than kinetic limitations. This multilevel redox activity, reinforced by the biogenic organic matrix, supports rapid electron-transfer kinetics, near-ideal pseudocapacitance, and minimal structural degradation during cycling. Collectively, the CV behavior of GF-MgO in PBS containing H_2O_2 demonstrates a synergistic combination of defect-mediated redox chemistry and organic-assisted charge storage, establishing GF-MgO as a promising electrode material for next-generation electrochemical sensing and energy-storage applications.

The electroactive surface area (A) of both the bare electrode and the *Gracilaria folifera*-functionalized MgO (GF-MgO) modified electrode has been calculated using the Randles-Sevcik equation based on cyclic voltammetry measurements.The Randles-Sevcik equation is given by:

$$I_p=(2.69\times10^5)\, n^{3/2}AD^{1/2}Cv^{1/2}$$

where
I_p is the peak current (A),
n is the number of electrons transferred (n = 1),
D is the diffusion coefficient (7.6×10^{-6} cm^2 s^{-1}),
C is the concentration (1 mM = 1×10^{-6} mol cm^{-3}), and
v is the scan rate (V s^{-1}).

The GF-MgO modified electrode (0.059 cm^2) showed a significantly higher surface area than the bare electrode (0.031 cm^2). This enhancement is attributed to increased surface roughness and additional active sites provided by MgO nanoparticles. The presence of oxygen vacancies and biofunctional groups further facilitates efficient electron transfer. Overall, the results confirm improved electrochemical performance of the GF-MgO modified electrode.

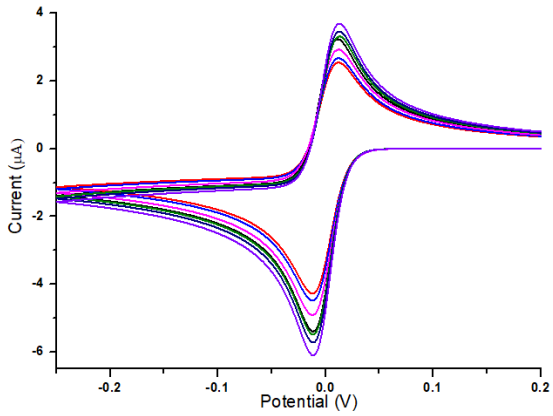

Figure 4. Cyclic voltammograms of the GF-MgO-modified electrode recorded in 0.1 M PBS containing H_2O_2 at different scan rates.

The enhanced redox peak currents and reduced peak separation observed for GF-MgO demonstrate improved electron transfer kinetics compared to pure MgO. This behavior is attributed to defect-induced energy states and the presence of bio-organic functional groups that facilitate charge transport. The quasi-reversible nature and high current response indicate strong pseudocapacitive characteristics, confirming that defect-engineered GF-MgO is highly suitable for electrochemical sensing and energy storage applications.

4.4. XPS Analysis

A detailed assessment of the surface chemical environment, oxidation states, and defect-level signatures of the *Gracilaria folifera*-mediated MgO nanoparticles was carried out using X-ray photoelectron spectroscopy (XPS), the results of which are shown in **Figure 5**. The survey spectrum spanning 0 to 1200 eV confirms a chemically simple surface composed exclusively of Mg, O, and C with no detectable contributions from metallic impurities or halides. Quantitative analysis reveals atomic percentages of Mg (32.6 at.%), O (52.8 at.%), and C (14.6 at.%), indicating oxygen-rich surface characteristics and the presence of bio-organic functional groups. The absence of additional elemental signals indicates that the biomolecules from *G. folifera* participate only as reducing and capping agents without incorporating foreign atoms into the MgO lattice[35].

The Mg 2p core-level spectrum exhibits a well-defined peak centered at ~49.4-50.2 eV, which corresponds to Mg^{2+} in stoichiometric magnesium oxide. This binding energy range is consistent with reported values for rock-salt MgO, confirming the complete oxidation of Mg during the green synthesis process. The narrow line shape and low full width at half maximum (FWHM) imply a uniform, chemically homogeneous Mg environment with minimal contributions from $Mg(OH)_2$ or surface $MgCO_3$ species. Any minor shift (<0.3 eV) relative to bulk MgO can be attributed to the presence of surface hydroxyl and carboxyl groups from the algal biomatrix, which induce slight perturbations in the local electron density around Mg^{2+}. The Mg 2s signal appearing near 88-90 eV further supports the predominance of Mg^{2+}, with no evidence of Mg^0 or sub-stoichiometric magnesium oxides (MgO_x, $x < 1$), which typically manifest at lower binding energies[36-38].

The O 1s spectrum shows two components: lattice oxygen (~530 eV) and surface hydroxyl/defect-related oxygen (~531-532 eV), indicating the presence of oxygen vacancies and surface functionalization (**Figure 5**). The major peak located at approximately 530.0-530.3 eV is assigned to lattice O^{2-} ions in stoichiometric MgO, confirming the presence of well-crystallized rock-salt magnesium oxide. In addition to this primary component, a broad shoulder appearing at higher binding energies (531.5-532.2 eV) reflects the contribution of surface-bound oxygen species, including hydroxyl groups (-OH), carbonyl and C-O functionalities derived from *G. folifera* polysaccharides and phenolic compounds, as well as oxygen associated with defect-rich regions. This higher-energy feature, along with the overall asymmetric line shape, indicates the presence of oxygen vacancies and surface hydroxylation, which introduce localized electronic states and modify the chemical environment of surface oxygen atoms. The coexistence of lattice oxygen and bio-organic oxygenated species

demonstrates that the nanoparticles possess a hybrid inorganic-organic surface, consistent with the FTIR results, and confirms that the *G. folifera* extract effectively functionalizes the MgO surface[39]. This surface chemical complexity is beneficial, as it enhances reactivity, promotes charge transfer, and improves the catalytic and biological performance of the biosynthesized MgO nanoparticles relative to pure MgO.

The C 1s spectrum exhibits three distinguishable components. The dominant peak at ~284.6-285.0 eV corresponds to adventitious carbon or aliphatic C-C/C-H moieties. A secondary peak at ~286.1-286.5 eV corresponds to C-O or C-OH functionalities, whereas the peak around 288.2-288.8 eV arises from carbonyl (C=O) or carboxylate (O-C=O) groups. These oxygenated carbon species are characteristic of biomolecules present in *G. folifera*, including sulfated galactans, amino acids, proteins, and phenolic derivatives. Their presence in the XPS spectra validates their role in stabilizing and capping the MgO nanoparticles. These surface molecular entities interact with MgO via coordination bonding, hydrogen bonding, and electrostatic interactions, thereby controlling the growth mechanism, nucleation kinetics, and final morphology[40].

The combined XPS results not only confirm the formation of pure MgO nanoparticles but also distinctly highlight the strong interfacial coupling between MgO and algal phytochemicals. This biogenic interface induces mild electronic perturbations, increases the density of surface hydroxyl groups, and stabilizes surface defects, all of which profoundly influence functional properties. The presence of hydroxyl- and carbonyl-rich biomolecular groups enhances surface reactivity, promotes charge transfer during electrochemical processes, and enables better adsorption of bacterial membranes during antibacterial assays. Moreover, such functionalization increases the dielectric constant by modulating interfacial polarization and space-charge effects.

The XPS results confirm Mg in the +2 oxidation state along with lattice oxygen and surface-bound hydroxyl and carbon-based functional groups, indicating successful biofunctionalization and defect-rich surface characteristics.

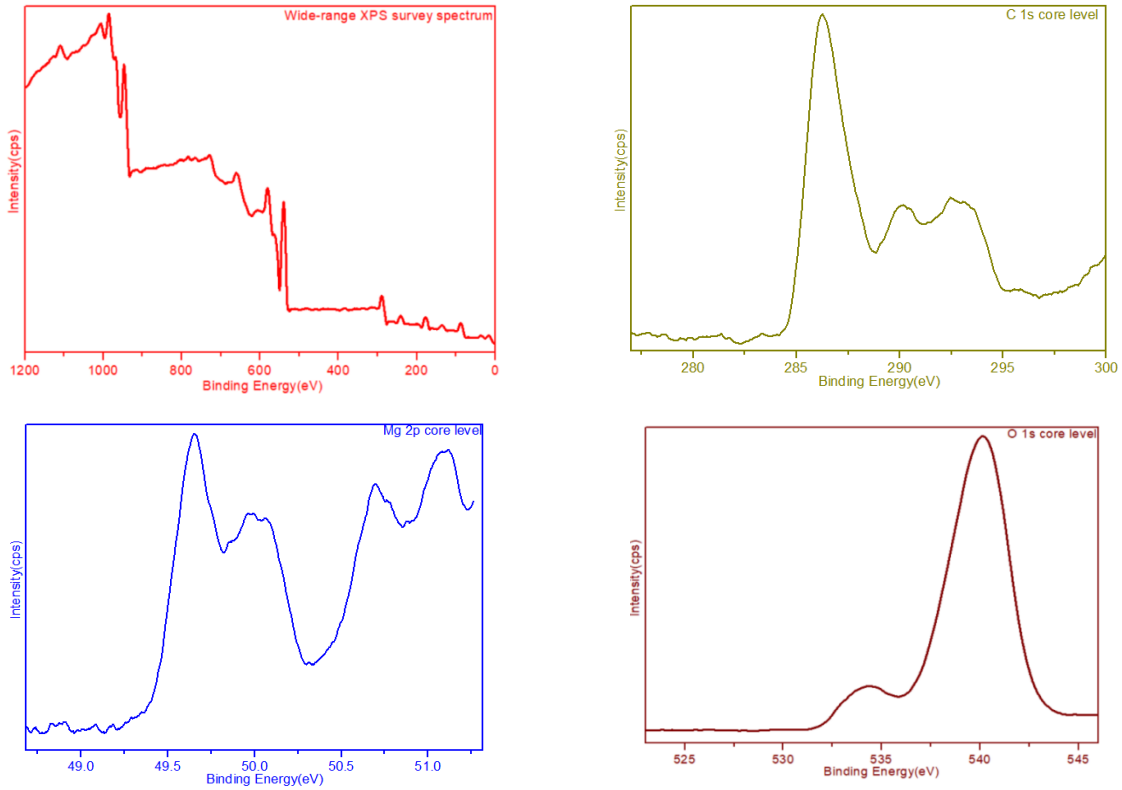

Figure 5. XPS survey and core-level spectra of GF-MgO nanoparticles.

4.5. Antidiabetic Activity

4.5.1. α -Amylase Inhibition Assay

The α-amylase inhibition activity of the synthesized samples was evaluated, and the results are presented in **Figure 6**. The assay measures the ability of the nanoparticles to suppress α-amylase, the key pancreatic enzyme involved in starch hydrolysis, thereby helping regulate postprandial glucose levels[41].

Nanoparticle suspensions of pure MgO and GF-MgO were prepared at concentrations of 20, 40, 60, 80, and 100 µg/mL. Each sample (1 mL) was mixed with 0.02 M sodium phosphate buffer (pH 6.9), 6 mM NaCl, and 250 µL of α-amylase solution, followed by incubation at 37 °C for 20 min. Afterward, 1% soluble starch was added and allowed to react for 20 min. The reaction was terminated by adding DNSA reagent, and the mixture was heated in a boiling water bath for 10 min. Absorbance was measured at 540 nm[42].

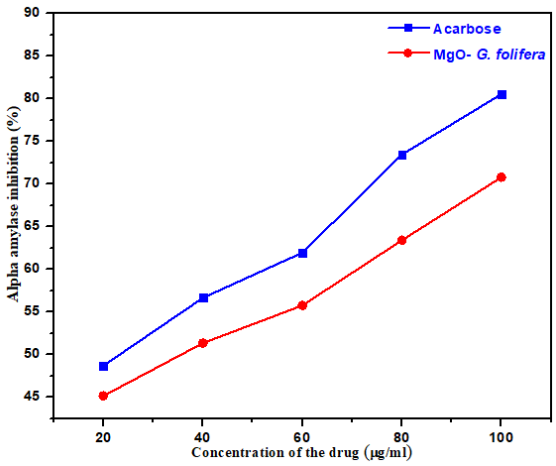

Figure 6. α-amylase inhibition : Comparative antidiabetic activity of MgO and GF-MgO nanoparticles.

Acarbose was used as the standard inhibitor.

The percentage of α-amylase inhibition was calculated using:

$$\% \, Inhibition = \frac{A_c - A_s}{A_c} \text{x } 100$$

Where A_C is the control absorbance (acarbose) and A_S is the sample absorbance. Consistent with **Figure 6**, both acarbose and GF-MgO show increasing inhibition with concentration. As expected, acarbose exhibits higher inhibition values, while GF-MgO shows strong but comparatively lower inhibition (45-71%).

4.5.2. α -Glucosidase Inhibition Assay

The α-glucosidase inhibition activity of MgO and GF-MgO nanoparticles was evaluated to assess their ability to suppress intestinal α-glucosidase, the enzyme responsible for the final step of carbohydrate digestion[43-45]. The results are shown in **Figure 7**.

Nanoparticle suspensions (20-100 µg/mL) were mixed with 0.1 M sodium phosphate buffer (pH 6.9), 6 mM NaCl, and 0.1 U of α-glucosidase, followed by incubation at 37 °C for 20 min. Subsequently, 500 µL of 2 mM p-nitrophenyl-α-D-glucopyranoside (pNPG) was added as the substrate. The reaction was stopped using 0.1 M sodium carbonate, and absorbance was measured at 405 nm. Acarbose served as the standard inhibitor. The inhibition percentage was calculated using the same formula described above. As depicted in **Figure 7**, GF-MgO displays concentration-dependent inhibition (37-73%), while acarbose consistently shows higher inhibition values (45-81%).

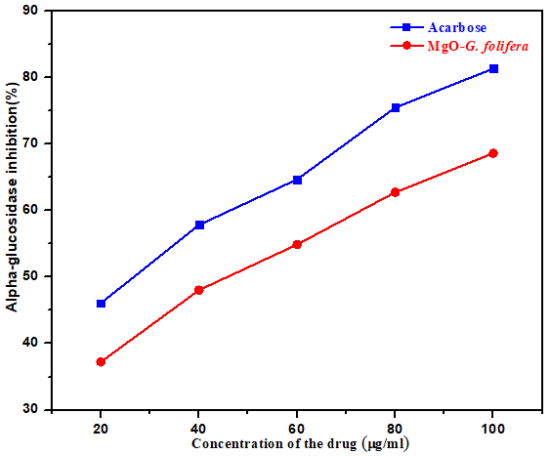

Figure 7. α-glucosidase inhibition at varying concentrations (20-100 µg/mL) in comparison with acarbose.

4.5.3. Antidiabetic Activity - Comparative Discussion

The comparative antidiabetic performance of MgO and GF-MgO nanoparticles, as illustrated in **Figures 6** and **7**, reveals a clear concentration-dependent increase in the inhibition of both α-amylase and α-glucosidase. GF-MgO consistently exhibits higher inhibitory activity than pure MgO across all tested concentrations, demonstrating the beneficial effect of algal functionalization[46]. In the α-amylase assay, the GF-MgO nanocomposite shows a progressive rise in inhibition with increasing concentration, reflecting stronger interactions between the algal-derived phytochemicals and the enzyme's active site; although acarbose displays higher inhibition overall, GF-MgO presents significant natural inhibitory potential. A similar enhancement is observed in the α-glucosidase assay, where GF-MgO again outperforms pure MgO due to the presence of bioactive moieties such as sulfated polysaccharides, phenolics, and flavonoids, which augment enzyme-binding affinity. The improved antidiabetic activity of GF-MgO arises from the synergistic interplay between MgO nanoparticles and algal phytochemicals, facilitating stronger hydrogen bonding and electrostatic interactions, enhanced active-site affinity, optimized surface charge modulation, and greater stabilization of enzyme-inhibitor complexes. Overall, the inhibition efficiency follows the order GF-MgO > Pure MgO, confirming the superior biological efficacy conferred by *G. folifera* functionalization.

To further highlight the significance of the present work, a comparison with previously reported MgO nanoparticles synthesized using different biological and chemical approaches is presented in **Table 3**.

Table 3. Comparative analysis of MgO nanoparticles synthesized using different approaches highlighting particle size, FTIR functional groups, and application performance.

Ref. No.	Source Material	Method	Particle Size (nm)	Key FTIR Functional Groups	Application
[47]	Red algae (*Gracilaria edulis*)	Green synthesis	18-42	O-H, C=O, C-O, sulfate	Antioxidant
[48]	Algal biomass	Phyco-synthesis	10-50	O-H, amide, phenolic, C-O-C	Biomedical
[49]	Brown seaweed extract	Green synthesis	25-60	O-H, C-H, C=O	Dye removal
[50]	Plant/biomass extract	Eco-friendly synthesis	20-55	O-H, C=O, C-O	Dye degradation, battery, sensor
[51]	Chemical precursors	Conventional synthesis	30-80	Metal-O, O-H	Catalysis
This Work	*Gracilaria foliifera*	Sol-gel + green route	~31-32	O-H, C-H, C=O, sulfate, C-O-C	Electrochemical + Antidiabetic

As shown in **Table 3**, the present GF-MgO nanoparticles exhibit comparable particle size with enhanced functional group diversity and improved electrochemical and antidiabetic performance. The combined effect

of green synthesis and defect engineering through *Gracilaria foliifera* provides superior functionality compared to previously reported systems.

5. Conclusion

In this work, defect-engineered MgO nanoparticles were successfully synthesized using *Gracilaria folifera* extract via a green sol-gel method. Structural analysis confirmed the formation of phase-pure cubic MgO with nanoscale crystallite size and high crystallinity, while FTIR and XPS results verified effective biofunctionalization through algal-derived biomolecules and enhanced oxygen-vacancy formation. Electrochemical studies demonstrated quasi-reversible redox behavior with significant pseudocapacitive contributions, indicating efficient defect-assisted charge transfer. Biologically, the synthesized GF-MgO nanoparticles exhibited superior antidiabetic activity compared to pure MgO, with lower IC_{50} values for α-amylase and α-glucosidase inhibition, attributed to synergistic interactions between MgO defect sites and bio-organic functional groups. Overall, the results confirm that *Gracilaria folifera*-mediated synthesis provides an effective strategy for producing multifunctional MgO nanomaterials with enhanced electrochemical and biomedical performance. The novelty of this work lies in the integration of green synthesis and defect engineering through *Gracilaria folifera*-mediated biofunctionalization, enabling the formation of defect-rich MgO nanoparticles with improved electrochemical activity and antidiabetic performance.

Funding statement

The authors received no specific funding for this study.

Conflicts of interest

The authors declare that they have no conflicts of interest to report regarding the present study.

Author contributions statement

Conceptualization, M.Adhithi, M. Yogeswari; Methodology, M. Yogeswari, M. Ehthishamul Haque; Investigation, M. Yogeswari; Resources, K.Dhanalakshmi, P.Sangeetha, B.Sangeetha; Writing, S. Sivakumar, B. Esther Bharathi. All authors have read and agreed to the published version of the manuscript.

Data availability statement

The datasets used and/or analysed during the current study available from the corresponding author on reasonable request.

References

1. Rotti, R.B., Sunitha, D.V., Manjunath, R., Roy, A., Mayegowda, S.B., Gnanaprakash, A.P., Alghamdi, S., Almehmadi, M., Abdulaziz, O., Allahyani, M. and Aljuaid, A., 2023. Green synthesis of MgO nanoparticles and its antibacterial properties. Frontiers in Chemistry, 11, p.1143614.
2. Soliman, M.K., Talib, A.H., Mahmoud, R., Ali, Z.A., Al-Haideri, H.H., Abalkhail, A., Binshaya, A.S., Salem, M.H., Al-Otibi, F.O. and Yassin, M.T., 2025. Ecofriendly magnesium oxide nanoparticles: anticancer, antimicrobial, and antidiabetic potentials in vitro. AMB Express, 15(1), pp.1-20.
3. Selim, S., Soliman, M.K., Almuhayawi, M.S., Alruhaili, M.H., Gattan, H.S., Saddiq, A.A., Hagagy, N., Alzahrani, A.J., Al Jaouni, S.K. and Salem, S.S., 2025. Green synthesis, characterization, molecular simulation, and in vitro biomedical application of magnesium oxide nanoparticles. PLoS One, 20(9), p.e0332367.
4. Krishna, B.V., Rao, P.T., Lakshmi, B.D., Vasudha, K., Basha, S.E., Kumar, B.P., Kiran, P.S.S., Chandra, K.S. and R.K., 2024. Green fabrication of *Tinospora cordifolia*-derived MgO nanoparticles: potential for diabetic control and oxidant protection. Next Materials, 3, p.100171.
5. Proniewicz, E., Vijayan, A.M., Surma, O., Szkudlarek, A. and Molenda, M., 2024. Plant-assisted green synthesis of MgO nanoparticles as a sustainable material for bone regeneration: spectroscopic properties. International Journal of Molecular Sciences, 25(8), p.4242.

6. Ansari, S.M., Saquib, Q., De Matteis, V., Awad Alwathnani, H., Ali Alharbi, S. and Ali Al-Khedhairy, A., 2021. Marine macroalgae display bioreductant efficacy for fabricating metallic nanoparticles: intra/extracellular mechanism and potential biomedical applications. Bioinorganic Chemistry and Applications, 2021, p.5985377.
7. Fatiqin, A., Amrulloh, H. and Simanjuntak, W., 2021. Green synthesis of MgO nanoparticles using *Moringa oleifera* leaf aqueous extract for antibacterial activity. Bulletin of the Chemical Society of Ethiopia, 35(1), pp.161-170.
8. Ramaraj, N., Thiripuranathar, G., Ekanayake, S., Attanayake, K. and Marapana, U., 2025. Phyco-synthesized inorganic nanoparticles and their biomedical applications. RSC Sustainability, 3(6), pp.2567-2581.
9. Shivappa, P., Gaddigal, A., Poojari, P., Irannanavar, K., Huyilagola, P., Irannanavar, S. and Kamanavalli, C., 2025. Green synthesis of magnesium oxide nanoparticles using *Gmelina arborea* leaf extract: antimicrobial, antioxidant, and antiangiogenic potentials. Materials NanoScience, 12(1), p.1184.
10. El-Sheekh, M.M., AlKafaas, S.S., Rady, H.A., Abdelmoaty, B.E., Bedair, H.M., Ahmed, A.A., El-Saadony, M.T., AbuQamar, S.F. and El-Tarabily, K.A., 2023. How synthesis of algal nanoparticles affects cancer therapy? A complete review. International Journal of Nanomedicine, 18, pp.6601-6638.
11. Chaudhary, R., Nawaz, K., Khan, A.K., Hano, C., Abbasi, B.H. and Anjum, S., 2020. Algae-mediated biosynthesis of nanoparticles and biomedical applications. Biomolecules, 10(11), p.1498.
12. Lithi, I.J., Nakib, K.I.A., Chowdhury, A.S. and Hossain, M.S., 2025. A review on the green synthesis of metal (Ag, Cu, Au) and metal oxide (ZnO, MgO, Co_3O_4, TiO_2) nanoparticles using plant extracts for antimicrobial applications. Nanoscale Advances, 7(9), pp.2446-2473.
13. Yang, Z. and Shen, J., 2025. Metal and metal oxide nanoparticles for environmental applications: a review. Nanoscale, 17(25), pp.15068-15085.
14. AlAbdulaal, T.H. and Abdullah, W., 2025. MgO nanoparticles improve structural, dielectric, and optical properties of polymer blends for optoelectronic applications. Results in Physics, p.108481.
15. Zaheer, I.E., Rehman, S.U., Liaquat, M., Saif, M., Kanval, F., Jehan, S., Ali, S., Alasmari, A., Alomrani, S.O., Al-Ashkar, I. and El Sabagh, A., 2026. Alleviation of tannery wastewater toxicity using metal oxide nanoparticles. Scientific Reports.
16. Abbas, S.F., Haider, A.J., Al-Musawi, S., Abbas, E.M., Alnayli, R.S., Taha, B.A., Choubani, M., Arsad, N. and Ibrahim, H.I., 2025. Optimizing wound healing with antibacterial metal oxide nanoparticles: comparative analysis of efficacy and mechanisms. Journal of Drug Delivery Science and Technology, 105, p.106563.
17. Devesa, S., 2025. Comparative overview of metal oxide nanoparticle synthesis methods: conventional sol-gel versus green approaches. Sol-Gel: A Versatile and Wide Technology.
18. Corrêa, L.E., Bordini, E.A.F., de Toledo Stuani, V., Álamo, L., Barra, R.H.D., Bronze-Uhle, E.S., Almeida, L.F., de Oliveira Fernandes, L., Andrade, C.A., de Almeida, J.M. and de Souza Costa, C.A., 2025. Bioactive photo-crosslinkable GelMA hydrogel incorporating metal oxide nanoparticles for bone tissue regeneration. Progress in Biomaterials, 14(4).
19. Kurhade, P., Kodape, S., Junghare, K., Bansod, P.G. and Bhutada, D., 2023. Development of MgO nanoparticles via green synthesis using mahua flower extract. Inorganic and Nano-Metal Chemistry, 53(3), pp.311-322.
20. Algotiml, R., Gab-Alla, A., Seoudi, R., Abulreesh, H.H., Ahmad, I. and Elbanna, K., 2022. Anticancer and antimicrobial activity of seaweed-mediated gold nanoparticles. Journal of Pure and Applied Microbiology, 16(1), pp.207-225.
21. Deo, H.A., Kanaskar, S.S., Zambare, M.S. and Kulkarni, N.M., 2025. MgO nanoparticles: synthesis, characterization and applications. IJSAT-International Journal on Science and Technology, 16(4).
22. Sivakumar, K., 2017. Phycosynthesis of silver nanoparticles from *Gracilaria foliifera*. International Journal for Science and Advance Research in Technology, 3(2), pp.442-450.
23. Chauhan, D., Kumar, R., Thakur, N., Singh, M. and Kumar, K., 2024. Ocimum sanctum-mediated doped MgO nanoparticles for environmental remediation. Hybrid Advances, 6, p.100199.
24. Vargas, M.A., Rivera-Muñoz, E.M., Diosa, J.E., Mosquera, E.E. and Rodríguez-Páez, J.E., 2021. ZnO and Mg-doped ZnO nanoparticles: synthesis and dye removal. Ceramics International, 47(11), pp.15668-15681.
25. Sutapa, I.W., Wahab, A.W., Taba, P. and La Nafie, N., 2018. Sol-gel synthesis and structural analysis of MgO nanoparticles. Oriental Journal of Chemistry, 34(2), p.1016.
26. Socrates, G., 2001. Infrared and Raman characteristic group frequencies: tables and charts. 3rd ed. Wiley.
27. Khongthong, S., Theapparat, Y., Roekngam, N., Tantisuwanno, C., Otto, M. and Piewngam, P., 2021. Sulfated galactan from red seaweed *Gracilaria fisheri*. International Journal of Biological Macromolecules, 189, pp.705-714.
28. Abinaya, S. and Kavitha, H.P., 2023. MgO nanoparticles as antibacterial agents. ACS Omega, 8(6), p.5225.

29. Zhang, X., Gao, H., Jin, W., Huang, Y., Xu, J. and Cao, J., 2024. Oxygen-vacancy-enriched MgO/carbon composite electrocatalyst. Materials Today Energy, 43, p.101587.
30. Goyal, M., Pandey, S.K. and Bhatnagar, N., 2025. Electrochemical performance of MgO nanoparticles. RSC Advances, 15(31), pp.25209-25220.
31. Vafaee-Shahi, S., Shishehbore, M.R., Sheibani, A. and Tabatabaee, M., 2020. MgO-CNT modified electrode for dopamine detection. Journal of the Chinese Chemical Society, 67(7), pp.1201-1212.
32. Zhang, X., Tang, F., Wang, M., Zhan, W., Hu, H., Li, Y., Friend, R.H. and Song, X., 2020. Oxygen vacancies in metal oxides. Science Advances, 6(10), p.eaax9427.
33. Allah, A.F., Abdel-Khalek, A.A., El-Sherbeeny, A.M., Al Zoubi, W. and Abukhadra, M.R., 2023. Glauconite nanorods for dye removal. ACS Omega, 8(51), pp.49347-49361.
34. Shirzad Choubari, M., Rahmani, S. and Mazloom, J., 2023. $Mg_{0.5}Ni_{0.5}Fe_2O_4$ nanospinels for electrochemical applications. Scientific Reports, 13(1), p.7822.
35. Podstawka-Proniewicz, E., Vijayan, A.M., Surma, O., Szkudlarek, A. and Molenda, M., 2023. Green synthesis of MgO nanoparticles. SSRN Electronic Journal, p.4593148.
36. Radulescu, D.M., Neacsu, I.A., Vasile, B.S., Surdu, V.A., Oprea, O.C., Trusca, R.D., Chircov, C., Popescu, R.C., Ilie, C.I., Ditu, L.M. and Drumea, V., 2025. Green MgO nanoparticles: antimicrobial applications. International Journal of Molecular Sciences, 26(18), p.9021.
37. Al-Harbi, L.M., Ezzeldien, M., Elhenawy, A.A. and Said, A.H., 2024. Bioinspired MgO nanoparticles from *Azadirachta indica*. Frontiers in Bioengineering and Biotechnology, 12, p.1480694.
38. Salunke, M.A., Wakure, B.S. and Wakte, P.S., 2023. FTIR analysis of *Gracilaria foliifera*. Research Journal of Pharmacy and Technology, 16(3), pp.1391-1394.
39. Panigrahi, T., Mukherjee, M., Palanisamy, M., Dadhich, A.S. and Pramanik, G., 2026. FTIR-based analysis of marine macroalgae. Regional Studies in Marine Science, p.104881.
40. Moghadam, K.R., Gharbi, S., Haddad-Mashadrizeh, A. and Yazdi, M.E.T., 2026. Green synthesis of gold nanoparticles using *Gracilaria gracilis*. Scientific Reports, 16, p.7427.
41. Gul, S., Arif, A., Siddiqui, N.N., Nawab, N., Tanoli, A.K., Ahmad, W. and Arif, A., 2025. Agar production from red algae. In: Global Conference on Green Construction Materials and Practices, pp.303-311.
42. Dhinesh, D., Ramanathan, S., Sagar, S. and Jeyaraj, G., 2025. Marine algae-derived nanocomposites for therapeutic applications.
43. Ezhilarasi, P. and Vanavil, B., 2023. Marine bacteria for curdlan production. Microbiology, 92(5), pp.725-733.
44. Palanisamy, J., Palanichamy, V.S., Vellaichamy, G., Perumal, P., Vinayagam, J., Gunalan, S., Prabhakaran, S.G., Thiraviam, P.P., Musthafa, F., Balaraman, A.K. and Rathinasamy, S., 2025. Green synthesis of silver nanoparticles from marine sources. Naunyn-Schmiedeberg's Archives of Pharmacology, 398(4), pp.3409-3432.
45. Aravinth, A., Mohan, P.K., Narayanan, M., Perumal, P., Dhanasundaram, S., Ramkumar, R., Kamaraj, C. and Rajaram, R., 2025. Silver nanoparticles from Gelidiella acerosa. Journal of Applied Phycology, 37(3), pp.2107-2119.
46. Aravinth, A., Pavithra, S., Kolandhasamy, P., Kamaraj, C., Rajaram, R. and Perumal, P., 2026. Silver nanoparticles from Amphiroa fragilissima. BioNanoScience, 16(2), p.97.
47. Rajiv, P., Gowtham, C. and Jeyapragash, D., 2022. Utilization of red algae *Gracilaria edulis* for bio-fabrication of MgO nanoparticles and antioxidant activity. JOM, 74(12), pp.4767-4771.
48. Ramaraj, N., Thiripuranathar, G., Ekanayake, S., Attanayake, K. and Marapana, U., 2025. Phyco-synthesized inorganic nanoparticles and their biomedical applications. RSC Sustainability, 3(6), pp.2567-2581.
49. Baghban, N., Jamali, M., Pourfadakari, S., Dobaradaran, S. and Yusefi, N., 2025. Green synthesis of MgO nanoparticles using brown seaweed extracts for dye removal. Chemical Engineering Communications, 212(1), pp.157-173.
50. Ramakrishna, L., Thippeswamy, R., Mallesh, G.K. and Kempahanumakkagari, S.K., 2024. Eco-friendly synthesis of MgO nanomaterials for dye degradation, battery, and sensor applications. Next Materials, 4, p.100193.
51. Dabhane, H., Ghotekar, S., Tambade, P., Pansambal, S., Oza, R. and Medhane, V., 2021. MgO nanoparticles: synthesis, characterization, and catalytic applications. European Journal of Chemistry, 12(1), pp.86-108.